Modelling thermo-acoustic instabilities of an anchored laminar flame in a simple lean premixed combustor: including hydrodynamic effects

Charles M. Luzzato* Raphael C. Assier† Aimee S. Morgans‡

Xuesong Wu§

Imperial College, London SW7 2AZ, United Kingdom

Lean premixed combustors reduce oxide of nitrogen (NO_x) emissions but are also prone to self sustained thermo-acoustic instabilities. Attempting to model these instabilities has become a popular research topic, and asymptotic based flame modelling allows us to capture all of the length scales involved in the instability. This paper presents a method for solving the full acoustic, hydrodynamic and flame coupling of an anchored laminar V-flame within a simple combustor. This allows us to model the Darrieus-Landau instability effects, and show how they influence the general behaviour and stability of the combustor when compared to G-Equation numerical results.

I. Introduction

The increased use of gas turbine engines has led to a growing concern regarding gas turbine emissions and pollution. Typical fuels used in combustion engines produce carbon, sulphur and oxides of nitrogen (NO_x) emissions, amongst others. Using lean premixed fuels, where the air to fuel ratio is much higher than stoichiometric conditions (low equivalence ratio), reduces the NO_x emissions of the combustor by reducing the flame temperature.[1] Unfortunately, for low values of equivalence ratio, a small change in equivalence ratio leads to a large change in local flame heat release. This makes premixed combustion systems very susceptible to combustions instabilities.[2]

Combustion instabilities are self sustained large amplitude flow oscillations caused by the coupling of combustor acoustics and unsteady heat release. The flame generates acoustic pressure waves which propagate within the combustion chamber and reflect on its extremities. They then propagate back to the flame and perturb the flame heat release which generates more pressure waves. According to the Rayleigh criterion, combustion instabilities occur when the incoming pressure wave at the flame is in phase with the heat release fluctuation.[3] These combustion instabilities lead to reduced combustion efficiency, and can have a detrimental effect on the structural integrity of the combustor.[4] Designing combustors which are guaranteed not to suffer from combustion instabilities is currently not possible. This has lead to a growing interest in both passive and active (feedback) control methods for suppression of instabilities.

Modelling of combustion instabilities requires, at the very least, a model for the flame response to acoustic waves, and a model for the propagation of acoustic waves within the combustor. One of the most popular approaches to modelling the flame is to use the G-Equation. The G-Equation model is a semi-empirical model which captures only kinematic effects of the flame. Furthermore, its usual implementation does not include any of the hydrodynamic effects occurring around the flame. For example, Darrieus-Landau instabilities are due to an interaction of the hydrodynamics around the flame, and the flame shape itself. They are caused by wrinkling of the flame due to curving streamlines on either side of the flame.[5] Because these effects occur in the hydrodynamic zone, they cannot be captured by the standard G-Equation implementation.

*Graduate Student, Department of Aeronautics, Imperial College.
†Research Associate, Department of Mathematics, Imperial College
‡Senior Lecturer, Department of Aeronautics, Imperial College
§Professor, Department of Mathematics, Imperial College

In the mathematics community, asymptotic expansion based flame modelling has been developed[6,7,8] over the past 40 years, assuming high activation energy and low Mach number. This approach is based on the idea that the combustor can be separated into different regions based on their respective length scales; these are the acoustic region, the hydrodynamic region and the flame region. At present, all these analyses are for flames which are freely convected within a combustor: they are not anchored. In this paper, we aim to export the approach to the classic problem of an anchored laminar flame within a simple combustor.

Bluff body anchored flame combustors are used in industrial boilers and heat recovery steam generators,[9] as well as ramjet and turbojet afterburners.[10] Typically, anchored flame combustor models include just an acoustic region and a combustion region. Incorporating and solving for the extra hydrodynamic region presents a new hurdle as the hydrodynamic flow is two dimensional, non-linear, and is coupled with the flame. However, under the assumption of small hydrodynamic amplitudes, the system of hydrodynamic equations can be reduced to one equation and one variable using spectral transformations, and solved in a semi analytical form. This method has been presented in Ref. 11, in the case of a freely propagating flame. Modelling an anchored flame, however, adds further complexity to the problem. In this case, the one dimensional acoustic field does not only have a convective action on the flame, but also causes deformation of the flame.

We present in this paper a new linearised asymptotic expansion based method for modelling bluff body anchored flames and hydrodynamic instabilities, including the Darrieus-Landau instability, based on the work of Wu and Moin.[11] There have already been some attempts to include the effects of hydrodynamics in combustor modelling, such as modelling the hydrodynamic effects around a propagating flame without acoustics Ref. 12. However, to the knowledge of the authors, this is the first attempt at modelling combustion instabilities in a way which fully accounts for the hydrodynamic features of the flow around the anchored flame, including the effects of hydrodynamics on the heat release.

II. Modelling Approach

The phenomena occurring in a long and thin combustor of length l, height h and infinite width involves very large length scales when studying acoustics, as well as very small length scales in the flame reaction process.[8] Because of this, the combustor can be divided, through asymptotic expansion, into separate regions based on their respective characteristic length scales, with compatibility conditions imposed at the boundaries. As such, we divide our combustor into an acoustic region, a hydrodynamic region, and a flame region,[8,7] as shown in figure 1 where the flame is anchored to a flame holder on the centreline of the duct.

- In the acoustic region, perturbations are entirely due to plane acoustic waves propagating at the speed of sound.[13] These leads to low frequency oscillations characterised by large lengths scales of order $\mathcal{O}\left(\frac{h}{M}\right)$, where the Mach number $M = \frac{u_{-\infty}}{\sqrt{\gamma p_{-\infty}/\rho_{-\infty}}}$ is small, and $u_{-\infty}$ and $\rho_{-\infty}$ are the pressure, velocity and density far upstream.

- The hydrodynamic region captures the two-dimensional effects of the flame on the flow, and has a length scale $\mathcal{O}(h)$.[8] The flow field in this region is the sum of plane acoustic waves and the two-dimensional hydrodynamic flow. To ensure compatibility, the hydrodynamic field converges to zero at the boundaries of the hydrodynamic and acoustic regions, and the acoustic field is assumed invariant due to the small relative size of the hydrodynamic region. The flame itself is represented by a simple discontinuity within the hydrodynamic region.[7]

- The flame region is the region in which the combustion process and thermal diffusion occur. Its characteristic length scale is the smallest of the three asymptotic regions and is of order $\mathcal{O}(d)$, with the intrinsic thickness of the flame given by the ratio of flame thermal diffusivity and the laminar steady flame velocity $d = \frac{D_{th}}{S_u}$. The flame region is used to derive the acoustic and hydrodynamic jumps across the flame from the equation of conservation of energy and the transport equation. These jumps will not be derived in this paper but can be found in Ref. 7 and Ref. 8.

The next sections will present the governing equations for each region. These will be given as a function of non-dimensional terms. We non-dimensionalise:

- The space variables (x, y) by the height of the combustion duct: $\frac{h}{2\pi}$.

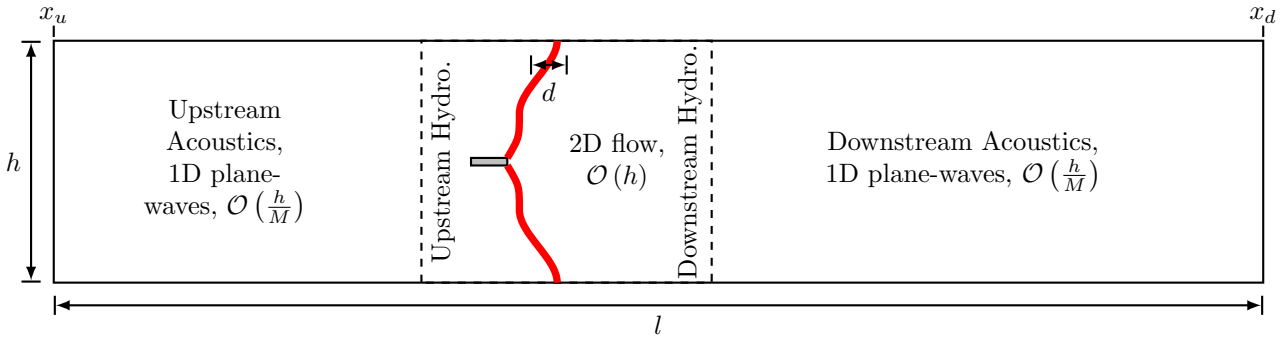

Figure 1. Diagram of the different combustor regions.

- The time t by the duct height over the steady laminar flame speed $\frac{h}{2\pi\bar{S}_u}$.
- The flow velocities $\mathbf{u} = (u, v)$ by the steady laminar flame speed $\bar{S}_u$. Note that the non-dimentionalisation could have been made with the mean flow $u^{\pm}$ since $\bar{S}_u$ and $u^{\pm}$ are of same order, but the choice of S_u was made to reduce the length of the equations.
- The density ρ by the mean flow density far upstream $\bar{\rho}_{-\infty}$.
- The temperature θ by the mean flow temperature far upstream $\bar{\theta}_{-\infty}$.
- We define the pressure as $p = p_{-\infty} + p^*\rho_{-\infty}\bar{S}_u^2$ where p^* is the non-dimensional pressure fluctuation which only captures the gauge pressure.[8]

II.A. Linearised acoustic region

The governing equations for the acoustic region are obtained from the general non dimensional conservation of mass and momentum equations using the following assumptions:

- The combustor is long and thin, so the plane wave assumption is valid
- The velocity, pressure and density variables can be linearised and written as the sum of a steady uniform mean, and a small fluctuation, such that we can write $u = \bar{u} + u_a$, $v = 0$, $p = \bar{p} + p_a$, and $\rho = \bar{\rho} + \rho_a$.
- Using an asymptotic expansion for small δ, where δ is the non dimensional flame thickness $\delta = \frac{2\pi d}{h}$, all terms of order $\mathcal{O}(\delta)$ are neglected, including the viscous effects.
- The flow in the acoustic region is assumed homentropic either side of the flame, and as such $p_a = c^2\rho_a$ where c is the celerity of sound.

Using the above assumptions, the obtained linearised acoustic equations are:

$$\begin{aligned} \frac{1}{c^2}\frac{\partial p_a}{\partial t} + \bar{\rho}^{\pm}\frac{\partial u_a}{\partial x} + \frac{\bar{u}}{c^2}\frac{\partial p_a}{\partial x} &= 0 \\ \bar{\rho}^{\pm}\left(\frac{\partial u_a}{\partial t} + \bar{u}^{\pm}\cdot\frac{\partial u_a}{\partial x}\right) &= -\frac{\partial p_a}{\partial x} \end{aligned} \tag{1}$$

These equations are valid in the acoustic region only, and can easily be solved using the method of characteristics.[14] The jump across the hydrodynamic region must still be determined to solve this system of equations across the flame.

II.B. Hydrodynamic region

To simplify the analysis of a moving flame discontinuity in the hydrodynamic region, the coordinate variables will be modified such that $(x, y, t) \to (\mathcal{G}, \eta, \tau)$, where $\mathcal{G} = x - \xi(y, t)$ and ξ defines the axial position of the flame, $y = \eta$ and $t = \tau$. With this change of variables, the flame discontinuity appears as a straight line in the hydrodynamic region, as shown in Fig. 2.

In previous works,[8,15,11] the configurations studied corresponded to freely propagating flames in a combustor. For those cases, the direct effects of acoustics on the flame was to modify the mean position of the flame in the duct. The thermo-acoustic coupling effect was then captured in the acoustic jump terms $[\![u_a]\!]$ and $\left[\!\left[\frac{\partial u_a}{\partial t}\right]\!\right]$present in the hydrodynamic governing equations and jumps.

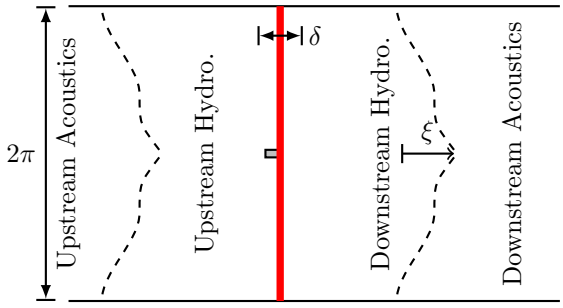

Figure 2. Diagram of the hydrodynamic region with modified coordinate variables

In the work presented here, the flame is anchored to a flame holder at a fixed point in the duct. In this configuration, the flame anchoring boundary condition is dependent on the acoustic perturbation at the flame. Therefore the acoustic perturbation participates in the deformation of the flame, and the thermo-acoustic coupling also occurs through the anchoring boundary condition.

Under these conditions, the governing equations for the hydrodynamic region are obtained from the general non-dimensional conservation of mass and momentum equations, using $(\mathcal{G}, \eta, \tau)$ coordinate variables and the following assumptions:

- Using asymptotic expansion, all terms of order $\mathcal{O}(\delta)$ are neglected. This leads to uniform density either side of the flame in the hydrodynamic region such that $\rho^- = \bar{\rho}^- = 1$ and $\rho^+ = \bar{\rho}^+ = \frac{1}{1+\bar{Q}}$,[16] where $\bar{\rho}$ is the non dimensional steady density in the acoustic region, and $\bar{Q}$ is the mean heat release at the flame.
- Using asymptotic expansion, all terms of order $\mathcal{O}(M)$ are neglected. In particular this means that in the hydrodynamic region, the convective terms of the acoustic equations are neglected.
- As discussed, fluctuations are caused by both hydrodynamic effects (which vary in space) and acoustic waves (which are assumed constant in this region either side of the flame). Because of the difference in length scales between the acoustic region of order $\mathcal{O}\left(\frac{1}{M}\right)$ and the hydrodynamic region of order $\mathcal{O}(1)$, the acoustic equations derived in Eq. (1) cannot directly be used in the hydrodynamic region. The correct length scale for the acoustics in the hydrodynamic region is given as $\tilde{\mathcal{G}} = M\mathcal{G}$. Thus to ensure compatibility between the two regions, a "stretching" is applied to the acoustic variables. This yields the general decomposition in the hydrodynamic region:[8,17]

$$\begin{aligned} u &= \bar{u}^{\pm} + u_a\left(0^{\pm}, t\right) + u_h\left(\mathcal{G}, \eta, t\right) \\ p &= \frac{1}{M} p_a\left(0, t\right) + \bar{p}^{\pm} + \frac{\partial p_a}{\partial \tilde{\mathcal{G}}}\left(0^{\pm}, t\right)\mathcal{G} + p_h\left(\mathcal{G}, \eta, t\right) + \frac{\partial p_a\left(0^{\pm}, t\right)}{\partial \tilde{\mathcal{G}}} \cdot \xi \\ v &= v_h\left(\mathcal{G}, \eta, t\right) \end{aligned} \tag{2}$$

The governing equations for continuity and conservation of momentum are finally given as:

$$\frac{\partial u_h}{\partial \mathcal{G}} + \frac{\partial v_h}{\partial \eta} = \frac{\partial v_h}{\partial \mathcal{G}} \cdot \frac{\partial \xi}{\partial \eta} \tag{3}$$

$$\bar{\rho}^{\pm}\left\{\frac{\partial u_h}{\partial t} + S\frac{\partial u_h}{\partial \mathcal{G}} + v_h \cdot \frac{\partial u_h}{\partial \eta}\right\} = -\frac{\partial p_h}{\partial \mathcal{G}} \tag{4}$$

$$\bar{\rho}^{\pm}\left\{\frac{\partial v_h}{\partial t} + S\frac{\partial v_h}{\partial \mathcal{G}} + v_h \cdot \frac{\partial v_h}{\partial \eta}\right\} = -\frac{\partial p_h}{\partial \eta} + \frac{\partial \xi}{\partial \eta}\frac{\partial p_h}{\partial \mathcal{G}} \tag{5}$$

where we have $S = \bar{u}^{\pm} + u_a\left(0^{\pm}, t\right) + u_h\left(\mathcal{G}, \eta, t\right) - v_h\left(\mathcal{G}, \eta, t\right) \cdot \frac{\partial \xi}{\partial \eta} - \frac{\partial \xi}{\partial t}$.

II.C. Flame region

The flame equation and jump conditions are derived from the analysis of the chemical species transport equation and the conservation of energy equation for a simple one step reaction. The flame equation involves flow variables evaluated just before the flame, and is given as:[16]

$$\frac{\partial \xi}{\partial t} = \bar{u}^- + u_a\big|_{0^-} + u_h\big|_{0^-} - v_h\big|_{0^-} \cdot \frac{\partial \xi}{\partial \eta} - \frac{S_u}{\bar{S}_u}\sqrt{1+\left(\frac{\partial \xi}{\partial \eta}\right)^2} \tag{6}$$

where S_u is the variable burning velocity, which is the sum of the laminar burning velocity $\bar{S}_u$ and a term of order $\mathcal{O}(\delta)$ responsible for the capturing the effects of flame curvature on laminar burning velocity.[7] This flame equation can be thought of as a modified G-Equation,[18] involving 2D hydrodynamics and variable burning velocity effects.

The hydrodynamic, acoustic, and steady jump equations across the flame are obtained from the study of the flame region[7,8] and are given by:

$$[p_h] = -\left[\!\left[\frac{\partial p_a}{\partial \tilde{\mathcal{G}}}\right]\!\right] \cdot \xi, \quad [u_h] = \bar{Q}\left\{\frac{1}{\sqrt{1+\left(\frac{\partial \xi}{\partial \eta}\right)^2}} - \left\langle\sqrt{1+\left(\frac{\partial \xi}{\partial \eta}\right)^2}\right\rangle_\eta\right\}, \quad [v_h] = \frac{-\bar{Q}\frac{\partial \xi}{\partial \eta}}{\sqrt{1+\left(\frac{\partial \xi}{\partial \eta}\right)^2}} \tag{7}$$

$$[\![p_a]\!] = 0, \qquad [\![u_a]\!] = \bar{Q}\left(\left\langle\sqrt{1+\left(\frac{\partial \xi}{\partial \eta}\right)^2}\right\rangle_\eta - \left\langle\sqrt{1+\left(\frac{\partial \bar{\xi}}{\partial \eta}\right)^2}\right\rangle_\eta\right) \tag{8}$$

$$[\bar{u}] = \bar{Q}\left\langle\sqrt{1+\left(\frac{\partial \xi}{\partial \eta}\right)^2}\right\rangle_\eta, \qquad [\bar{p}] = -\bar{Q} \tag{9}$$

where the jumps across the flame region are indicated as $[a] = a^+ - a^-$, and $[\![a]\!]$ is used for acoustic jumps. Furthermore $\langle a\rangle_\eta$ indicates the average over η, and $\bar{\xi}$ is the steady flame shape. Equations (3) – (5) are fully non-linear, and solving them coupled with Eq. (7)– (9) and Eq. (6) presents an difficult challenge. The next section will consider a linearisation of these equations which can be solved semi-analytically.

III. Semi analytical method for solving the linearised hydrodynamic equations using spectral methods

We have presented the equations governing each region. In the case of the acoustic region, the linearised acoustic equations can easily be solved either side of the flame using the method of characteristics.[14] However, relating the upstream and downstream acoustic regions, whilst solving the coupled two dimensional non-linear hydrodynamic equations, is more involved. Indeed, the acoustic fields depends on the values of the acoustics jumps across the hydrodynamic region, and the hydrodynamic fields depend on the values of the hydrodynamic jumps across the flame region. Similarly, the shape of the flame, which defines the values of the jumps, depends on the acoustic and hydrodynamic fields. Therefore, solving the acoustics and hydrodynamics in the presence of the flame is a fully coupled non-linear problem.

III.A. Linearisation

In order to simplify the governing equations, let us make to the following assumptions:

- The acoustic field is weak, and so $|(u_a, p_a)| << 1$; this is the same assumption that was used in the linearised acoustic model[19] and is valid until the flame moves upstream of the flame holder (flashback).[20]
- The hydrodynamic motion is weak, and so $|(u_h, v_h, p_h)| << 1$.[15] For a flame with a slope of order $\mathcal{O}(1)$, this is not strictly true at the wall, as it will impose $v_h \neq 0$ there.
- The flame position can be expressed as $\xi = \bar{\xi}(\eta) + \xi'(\eta, t)$, where the overbar denotes the steady value, and the apostrophe denotes the fluctuation, where we assume that $\xi'(\eta, t) << 1$.
- There are no vortical disturbances in the incoming flow.

These assumptions allow us to linearise the hydrodynamic equations (3)–(5) and jump equations (7); this linearisation procedure however is dependent on the mean flow parameters which determine the steady flame shape, as is explained in the next section.

III.A.1. Flame shape linearisation

The choice of flame shape linearisation requires further consideration. Let us assume that the small acoustic and hydrodynamic fluctuations impose a small flame shape fluctuation ξ'; however, nothing has been assumed so far for the order of the magnitude of the steady flame shape.

To see what assumptions must be made about the steady flame shape in order to solve the problem semi-analytically, we decompose the slope of the flame as $\frac{\partial \xi}{\partial \eta} = \frac{\partial \bar{\xi}}{\partial \eta} + \frac{\partial \xi'}{\partial \eta}$. From Eq. (6), the steady flame equation can be written as:

$$\bar{u} + \bar{u}_h\big|_0 - \bar{v}_h\big|_0 \cdot \frac{\partial \bar{\xi}}{\partial \eta} - \sqrt{1 + \left(\frac{\partial \bar{\xi}}{\partial \eta}\right)^2} = 0 \tag{10}$$

and hence:

$$\frac{\partial \bar{\xi}}{\partial \eta} = \frac{-\bar{v}_h\big|_0 \bar{u} - \bar{u}_h\big|_0 \bar{v}_h\big|_0 \pm \sqrt{-1 + \bar{u}^2 + 2\bar{u}_h\big|_0 \bar{u} + \bar{u}_h\big|_0^2 + \bar{v}_h\big|_0^2}}{1 - \bar{v}_h\big|_0^2} \tag{11}$$

where the $\mathcal{O}(\delta)$ term has been deliberately neglected, and all variables are upstream ($^-$) variables. This yields the linearised solution for the steady flame slope, where the steady hydrodynamic variables are assumed small compared to the laminar flame speed and $\bar{u}^- \neq 1$:

$$\frac{\partial \bar{\xi}}{\partial \eta} = -\bar{v}_h\big|_0 \bar{u} \pm \frac{\bar{u}_h\big|_0 \bar{u}}{\sqrt{\bar{u}^2 - 1}} \pm \sqrt{\bar{u}^2 - 1} \tag{12}$$

From Eq. (12), it is clear that the steady flame shape can be separated into two terms that we write $\mathcal{C} = \pm\sqrt{\bar{u}^2 - 1}$ and $\tilde{\mathcal{C}} = \pm\frac{\bar{u}_h \bar{u}}{\sqrt{(\bar{u})^2 - 1}} - \bar{v}_h \bar{u}$. The first term $\mathcal{C}$ is of order $\mathcal{O}(\bar{u}^-)$ and is constant along η. The same constant slope is obtained with the G-Equations in Ref. 13 and Ref. 21 from the ratio of mean flow and laminar flame speed, and bears good agreement with experimental results. The second term $\tilde{\mathcal{C}}(\eta)$ is small and arises from the presence of a hydrodynamic flow field. We can now re-express our flame slope as $\frac{\partial \xi}{\partial \eta} = \mathcal{C} + \tilde{\mathcal{C}}(\eta) + \frac{\partial \xi'}{\partial \eta}(\eta, t)$ for our linearisation process.

Depending on the order of magnitude of the mean flow $\bar{u}^-$, two different linearisation procedures can be used.

- In the first case, $\bar{u}^-$ is of order $\mathcal{O}(1)$ and is greater than 1. The steady flame is close to horizontal and so $\mathcal{C}$ is of order $\mathcal{O}(1)$; this configuration is commonly known as the V-flame shape. This is fundamentally different from the method presented in Ref. 11 (where the steady flame shape could be assumed to be small) and induces further difficulties when solving the hydrodynamic field. In particular, it imposes that $\bar{Q} << 1$ and that $v_h \neq 0$ at the wall. This may turn out to be restrictive for industrial configurations, but will serve as a validation for more complicated numerical methods which relax the assumption.

- In the second case, $\bar{u}^- \approx 1$, and therefore the steady flame shape is close to vertical such that $\mathcal{C} << 1$. This is the configuration used in Ref. 11, and does not impose any restrictions on the mean heat release rate $\bar{Q}$. In the rest of this paper, this case will be referred to as the flat flame case.

Note that when $\bar{u}^- = 1$, the linearisation of the flame equation takes a slightly modified form and yields:

$$\frac{\partial \bar{\xi}}{\partial \eta} = -\bar{v}_h - \bar{u}_h\big|_0 \bar{v}_h\big|_0 \pm \sqrt{2\bar{u}_h\big|_0 + \bar{u}_h\big|_0^2 + \bar{v}_h\big|_0^2} \tag{13}$$

The above is used to linearise the hydrodynamic equations (3) – (5), and jumps (7).

III.A.2. Linearised hydrodynamics with a flat steady flame

From Eq. (12), the steady flame is obtained when $\bar{u}^- \approx 1$, or in dimensional terms when the mean flow is approximately equal to the steady laminar burning velocity of the flame $\bar{S}_u$. In this configuration, the steady flame gradient is small, and so $\bar{\xi}$ is small.

The hydrodynamic conservation equations (3) – (5) can then be linearised as:

$$\frac{\partial u_h}{\partial \mathcal{G}} + \frac{\partial v_h}{\partial \eta} = 0 \tag{14}$$

$$\bar{\rho}^{\pm}\left(\bar{u}^{\pm}\frac{\partial u_h}{\partial \mathcal{G}} + \frac{\partial u_h}{\partial t}\right) = -\frac{\partial p_h}{\partial \mathcal{G}} \tag{15}$$

$$\bar{\rho}^{\pm}\left(\bar{u}^{\pm}\frac{\partial v_h}{\partial \mathcal{G}} + \frac{\partial v_h}{\partial t}\right) = -\frac{\partial p_h}{\partial \eta} \tag{16}$$

where higher order terms have been neglected.

Similarly the jump equations across the flame Eq. (7) and Eq. (8) can be linearised as:

$$[p_h] = -\left[\!\left[\frac{\partial p_a\big|_{0^-}}{\partial \tilde{\mathcal{G}}}\right]\!\right] \cdot \xi \tag{17}$$

$$[u_h] = \bar{Q}\left[1 - \frac{1}{2}\left(\mathcal{C} + \tilde{\mathcal{C}} + \left(\frac{\partial \xi'}{\partial \eta}\right)\right)^2 - \left\langle 1 + \frac{1}{2}\left(\mathcal{C} + \tilde{\mathcal{C}} + \left(\frac{\partial \xi'}{\partial \eta}\right)\right)^2 \right\rangle_\eta\right] \tag{18}$$

$$[v_h] = -\bar{Q}\left(\mathcal{C} + \tilde{\mathcal{C}} + \left(\frac{\partial \xi'}{\partial \eta}\right)\right) \tag{19}$$

$$[\![u_a]\!] = \bar{Q}\left(\frac{1}{2}\left\langle \mathcal{C} + \tilde{\mathcal{C}} + \left(\frac{\partial \xi'}{\partial \eta}\right)\right\rangle_\eta - \frac{1}{2}\left\langle \mathcal{C} + \tilde{\mathcal{C}}\right\rangle_\eta\right) \tag{20}$$

$$[\![p_a]\!] = 0 \tag{21}$$

The hydrodynamic conservation equations and jump equations given here are exactly the same as seen in Ref. 15 and Ref. 11; the key difference comes from the boundary condition imposed at the flame base which will induce flame-acoustic coupling. The flame equation upon which the boundary condition will be imposed is given as:

$$\frac{\partial \xi}{\partial t} = u_a\big|_{0^-} + u_h'\big|_{0^-} - \frac{1}{2}\left(\tilde{\mathcal{C}} + \frac{\partial \xi'}{\partial \eta}\right)^2 - \mathcal{C}\left(\tilde{\mathcal{C}} + \frac{\partial \xi'}{\partial \eta}\right) + \delta M_a\left(\frac{\partial \tilde{\mathcal{C}}}{\partial \eta} + \frac{\partial^2 \xi'}{\partial \eta^2}\right) \tag{22}$$

Where M_a is the Markstein number. Note that the δ term is kept here as this term captures the curvature effects of the flame. It is also responsible for the preferential diffusion of large wavenumber Darrieus-Landau instabilities.[22]

III.A.3. Linearised hydrodynamics with a V-flame steady flame

In this case, $\bar{u}^- > 1$ and the constant slope flame obtained from the term $\mathcal{C}$ dominates and is of order $\mathcal{O}(1)$.

The hydrodynamics conservation equations can be linearised from Eq. (3) – (5) as:

$$\frac{\partial u_h}{\partial \mathcal{G}} + \frac{\partial v_h}{\partial \eta} = \mathcal{C}\frac{\partial v_h}{\partial \mathcal{G}} \tag{23}$$

$$\bar{\rho}^{\pm}\left(\bar{u}^{\pm}\frac{\partial u_h}{\partial \mathcal{G}} + \frac{\partial u_h}{\partial t}\right) = -\frac{\partial p_h}{\partial \mathcal{G}} \tag{24}$$

$$\bar{\rho}^{\pm}\left(\bar{u}^{\pm}\frac{\partial v_h}{\partial \mathcal{G}} + \frac{\partial v_h}{\partial t}\right) = -\frac{\partial p_h}{\partial \eta} + \mathcal{C}\frac{\partial p_h}{\partial \mathcal{G}} \tag{25}$$

Similarly the jump equations across the flame can be linearised from Eq. (7) and Eq. (8) as:

$$[p_h] = -\left[\!\left[\frac{\partial p_a(0^{\pm},t)}{\partial \mathcal{G}}\right]\!\right]\cdot\bar{\xi} \tag{26}$$

$$[u_h] = \bar{Q}\left[\frac{1}{\sqrt{1+\mathcal{C}^2}} - \frac{\mathcal{C}\frac{\partial\xi'}{\partial\eta}+\mathcal{C}\tilde{\mathcal{C}}}{(1+\mathcal{C}^2)\sqrt{1+\mathcal{C}^2}} - \left(\left\langle\sqrt{1+\mathcal{C}^2}+\frac{\mathcal{C}\frac{\partial\xi'}{\partial\eta}+\mathcal{C}\tilde{\mathcal{C}}}{\sqrt{1+\mathcal{C}^2}(1+\mathcal{C}^2)}\right\rangle_{\eta}\right)\right] \tag{27}$$

$$[v_h] = \frac{-\bar{Q}\left(\mathcal{C}+\tilde{\mathcal{C}}+\frac{\partial\xi'}{\partial\eta}+\mathcal{C}^3\right)}{(1+\mathcal{C}^2)\sqrt{1+\mathcal{C}}^2} \tag{28}$$

$$[\![u_a]\!] = \bar{Q}\left(\frac{\mathcal{C}\left\langle\frac{\partial\xi'}{\partial\eta}\right\rangle_{\eta}}{\sqrt{1+\left(\frac{\partial\bar{\xi}}{\partial\eta}\right)^2}}\right) \tag{29}$$

$$[\![p_a]\!] = 0 \tag{30}$$

The jump equations (27) – (28) show that for the hydrodynamics to be small when $\mathcal{C}$ is of order $\mathcal{O}(1)$, we must have $\bar{Q} << 1$. This is a drawback of this case, and stems from the requirement that the steady and fluctuating hydrodynamic fields be small. Finally, the fluctuating flame shape is given as:

$$\frac{\partial\xi'}{\partial t} = u_a\big|_{0^-} + u_h\big|_{0^-} - v_h\big|_{0^-}\cdot\mathcal{C} - \mathcal{C}\frac{\tilde{\mathcal{C}}+\frac{\partial\xi'}{\partial\eta}}{\sqrt{1+\mathcal{C}^2}} + \delta M_a\left(\frac{\partial\tilde{\mathcal{C}}}{\partial\eta}+\frac{\partial^2\xi'}{\partial\eta^2}\right) \tag{31}$$

III.B. Spectral transformation

III.B.1. Premise

The acoustics shown in Eq. (1) can be solved analytically using the method of characteristics. Furthermore a forward time marching solution will be used to determine the time varying flame shape ξ from the appropriate linearised form of Eq. (6). By expressing the variables with a dependency on η using Fourier series, it is possible to reduce the system of three equations governing the hydrodynamics (Eq. (23)–(25) or Eq. (14)–(16)) to just one equation involving one spectral variable at $\mathcal{G} = 0^{\pm}$. This method was proposed by Ref. 11 and implemented with acoustic coupling by Ref. 23 for a freely propagating flame, and will be adapted here for our anchored flame configuration.

To derive the spectral equation, the variables dependent on η are written as Fourier series:

$$u_h(\mathcal{G},\eta,t) = \sum_{n=-\infty}^{\infty}\widehat{u_h}_n(t,\mathcal{G})\,e^{in\eta}, \quad v_h(\mathcal{G},\eta,t) = \sum_{n=-\infty}^{\infty}\widehat{v_h}_n(t,\mathcal{G})\,e^{in\eta}$$
$$p_h(\mathcal{G},\eta,t) = \sum_{n=-\infty}^{\infty}\widehat{p_h}_n(t,\mathcal{G})\,e^{in\eta} \qquad \xi(\eta,t) = \sum_{n=-\infty}^{\infty}\hat{\xi}_n(t)\,e^{in\eta} \tag{32}$$

where $n \in \mathbb{Z}$ since our duct is periodic in η with period 2π. Only the top half of the duct is solved for to avoid convolutions. This leads to problems with taking the Fourier series of a non-periodic signal, which is solved through the use of signal extension methods with Tikhonov regularization.[24] It will be shown that the governing hydrodynamic equations can be linearised in such a way that the hydrodynamic solutions can be found for each wave-number.

III.B.2. Derivation in the V-flame case

The series shown in Eq. (32) are inserted into the hydrodynamic equations shown in Eq. (23)–(25). Using a method similar to that presented in Ref. 15, we can express all hydrodynamic variables as a function of the unknown variable ϕ (which takes different values of ϕ^- and ϕ^+ upstream and downstream of the flame respectively):

$$\widehat{u_{hn}}\left(t,\mathcal{G}\right)=\begin{cases}\phi_n^-\left(t\right)e^{\mathcal{K}_n^-\mathcal{G}} & \text{for } \mathcal{G}<0\\ \phi_n^+\left(t\right)e^{-\mathcal{K}_n^+\mathcal{G}}+C_n^+\left(t\right) & \text{for } \mathcal{G}>0\end{cases} \tag{33}$$

$$\widehat{v_{hn}}\left(t,\mathcal{G}\right)=\begin{cases}\frac{in-\mathcal{C}\mathcal{K}_n^-}{\mathcal{K}_n^-}\phi_n^-\left(t\right)e^{\mathcal{K}_n^-\mathcal{G}} & \text{for } \mathcal{G}<0\\ -\frac{in+\mathcal{C}\mathcal{K}_n^+}{\mathcal{K}_n^+}\phi_n^+\left(t\right)e^{-\mathcal{K}_n^+\mathcal{G}}+D_n^+\left(t\right) & \text{for } \mathcal{G}>0\end{cases} \tag{34}$$

$$\widehat{p_{hn}}\left(t,\mathcal{G}\right)=\begin{cases}-\frac{\bar{\rho}^-\left(\frac{\partial\phi_n^-(t)}{\partial t}+\mathcal{K}_n^-\bar{u}^-\phi_n^-(t)\right)e^{\mathcal{K}_n^-\mathcal{G}}}{\mathcal{K}_n^-} & \text{for } \mathcal{G}<0\\ \frac{\bar{\rho}^+\left(\frac{\partial\phi_n^+(t)}{\partial t}-\mathcal{K}_n^+\bar{u}^+\phi_n^+(t)\right)e^{-\mathcal{K}_n^+\mathcal{G}}}{\mathcal{K}_n^+} & \text{for } \mathcal{G}>0\end{cases} \tag{35}$$

where $\mathcal{K}_n^-=\frac{n}{\mathcal{C}^2+1}(1+i\mathcal{C})$ and $\mathcal{K}_n^+=-\frac{n}{\mathcal{C}^2+1}(i\mathcal{C}-1)$.

Equations (33)–(35) can now be substituted into the hydrodynamic jumps Eq. (26)–(28) and the conservation equations Eq. (23)–(25) expressed at the flame $\mathcal{G}=0$. By assuming no vortical disturbances in the upstream hydrodynamics, a well defined system of equations is obtained, and can be rearranged to express the partial differential equation governing $\frac{\partial\phi_n^-}{\partial t}$ when $n\neq 0$.

$$\frac{\partial\phi_n^-}{\partial t}=-\frac{i\phi_n^-\left(n\bar{\rho}^-\bar{u}^-+n\bar{\rho}^+\bar{u}^+\right)}{\left(i+\mathcal{C}\right)\left(\bar{\rho}^-+\bar{\rho}^+\right)}-\frac{i\left(-\epsilon n+\left(\mathcal{C}\frac{\partial\beta}{\partial t}+\frac{\partial\lambda}{\partial t}\right)\bar{Q}\bar{\rho}^++i\beta n\bar{Q}\bar{\rho}^+\bar{u}^+\right)}{\left(i+\mathcal{C}\right)\left(\bar{\rho}^-+\bar{\rho}^+\right)} \tag{36}$$

where β, λ and ϵ stem from the jump equations Eq. (26)–(27) such that

$$\beta=\frac{in\widehat{\xi}_n}{(1+\mathcal{C}^2)\sqrt{1+\mathcal{C}}^2} \tag{37}$$

$$\lambda=\frac{\mathcal{C}in\widehat{\xi}_n}{(1+\mathcal{C}^2)\sqrt{1+\mathcal{C}^2}}-\left\langle\frac{\mathcal{C}in\widehat{\xi}_n}{\sqrt{1+\mathcal{C}^2}(1+\mathcal{C}^2)}\right\rangle_\eta \tag{38}$$

$$\epsilon=\mathcal{F}_n\left(-\left[\!\left[\frac{\partial p_a}{\partial\mathcal{G}}\right]\!\right]\cdot\bar{\xi}\right) \tag{39}$$

where $\mathcal{F}_n\left(b\right)$ indicates the coefficient n of the Fourier series representation of b.

III.B.3. Derivation of the flat flame case

The same procedure is used in the flat flame case. This derivation will yield the same equations as obtained in Ref. 11 albeit with entropy and gravity neglected and the hydrodynamic velocity jump $[\widehat{u_h}]$ conserved. These results will not be explained here and are only given for the sake of completeness. As such the final governing equation for $\frac{\partial\phi_n^-}{\partial t}$ is given as:

$$\frac{\partial\phi_n^-}{\partial t}=-\frac{\phi_n^-\left(n\bar{\rho}^-\bar{u}^-+n\bar{\rho}^+\bar{u}^+\right)}{\bar{\rho}^-+\bar{\rho}^+}-\frac{-\epsilon n+\frac{\partial\lambda}{\partial t}\bar{Q}\bar{\rho}^++n\beta n\bar{Q}\bar{\rho}^+\bar{u}^+}{\bar{\rho}^-+\bar{\rho}^+} \tag{40}$$

where β, λ and ϵ stem from the jump equations Eq. (17)–Eq. (18) such that

$$\beta=in\widehat{\xi} \tag{41}$$

$$\lambda=\mathcal{F}_n\left(\frac{1}{2}\left(\mathcal{C}+\tilde{\mathcal{C}}+\left(\frac{\partial\xi'}{\partial\eta}\right)\right)^2-\left\langle\frac{1}{2}\left(\mathcal{C}+\tilde{\mathcal{C}}+\left(\frac{\partial\xi'}{\partial\eta}\right)\right)^2\right\rangle_\eta\right) \tag{42}$$

$$\epsilon=\mathcal{F}_n\left(-\left[\!\left[\frac{\partial p_a}{\partial\mathcal{G}}\right]\!\right]\cdot\bar{\xi}\right) \tag{43}$$

Note that Eq. (36) reduces to Eq. (40) when $\xi<<1$.

III.C. Numerical implementation

The G-equation model is well established in the engineering community to compute thermo-acoustic instabilities.[25] We shall therefore try and conserve some elements of the G-equation solver when implementing the computation of the hydrodynamic field.

In the case of the G-equation, the flame shape is computed every time step in the physical domain. This gives a new flame shape, from which the new hydrodynamic variables and acoustic waves could be obtained. However, for our new model, the hydrodynamic variables must be solved in the spectral domain. This means that their spectral form must be determined at each time step in order to compute the new hydrodynamic solutions. Once the new hydrodynamic solutions have been obtained in spectral space, they must be converted back to physical space to move on to the next iteration. This procedure is shown in figure 3, and can be summarised as follows:

- Start from an initial flame shape, and compute the acoustic pressure waves using Eq. (1).
- Reconstruct the acoustic velocity at the flame using the method of characteristics.
- Find the Fourier series coefficients of the flame shape, and the initial hydrodynamic field, as shown in Eq. (32)
- Compute the new value of ϕ using Eq. (36) or Eq. (40) using a simple finite difference scheme.
- Transform the new hydrodynamic variables back to Cartesian space with Eq. (32)
- Use the newly obtained hydrodynamic fields, and the acoustic velocity field, to generate u_{gutter}
- Obtain the new flame shape using equation Eq. (6) and a second numerical scheme.[26]

The process is repeated for each time step. It is interesting to note that when the spectral space section of figure 3 is ignored, the method reduces to the standard G-equation implementation.

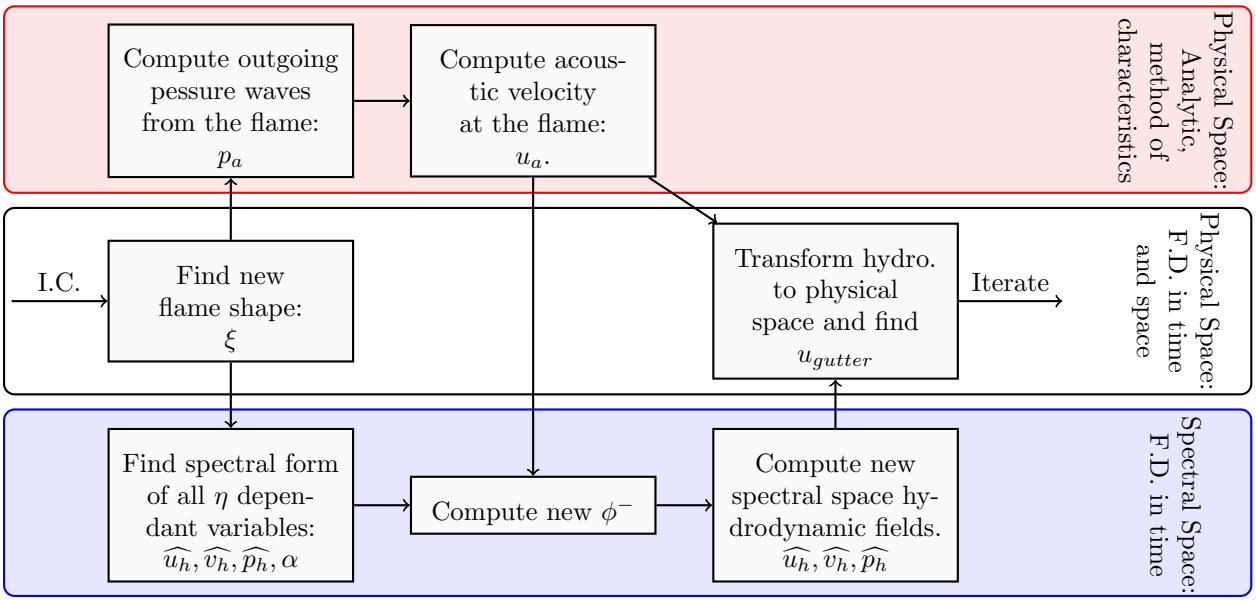

Figure 3. Diagram of the numerical implementation.

III.D. Numerical Schemes

As mentioned, there are two finite different schemes used in this new model.

Flame Shape P.D.E. The first numerical scheme is used to compute the new flame shape, and uses a finite difference method in space and time. A simple first order forward time marching Euler method is used, alongside a first order forward difference in space. This proves stable for an adequate choice of time step and spatial grid, even though the numerical scheme could easily be improved.

Hydrodynamics P.D.E. The second numerical scheme is used to compute the new variable ϕ^-, and therefore uses a finite difference method in time only, as space is handled in the spectral domain. The same first order forward time marching Euler method is used.

An approximation of the hydrodynamic variables must also be made in our simulation. Indeed, when solving only the top half of the duct, a signal extension is applied to ensure that the variables for which we write the Fourier series remain periodic in a larger domain. This is done done by solving a system of linear equations, and is subject to large errors when the signal to be transformed is not smooth, as can sometimes be the case around the anchoring point of the flame.

IV. Results

The following section presents preliminary results obtained with the new model and compared to G-Equation simulations. As explained previously, he G-Equation model is a non-linear kinematic model commonly used in engineering. It requires some empirical measurements, but usually bears good agreement with experiments.[13,26] It does not, however, capture any of the hydrodynamic effects of the flame, and is therefore limited to modelling only flame-acoustic interactions.

IV.A. Stable Configuration

A simulation was run with the G-Equation model and the parameters shown in table 1, where the reflection coefficients at the upstream and downstream boundaries are given as R_u and R_d. Note that the heat release chosen here is very low to verify the linearisation conditions imposed on $\bar{Q}$.

Table 1. Combustor parameters for the comparison to the G-Equation results in the stable case.

$h/2$ [cm]	x_u[m]	x_d[m]	x_{ref}[m]	R_u	R_d	M	δx [mm]	δt [ms]	Flame angle [°]	$\bar{Q}/\theta_{-\infty}$
3	-1.2	0.799	0.118	1	-1	0.02	0.236	0.02	8.627	0.075

The reflection coefficients where chosen specifically such that no flame-acoustic instability developed. Once the energy from the initial low amplitude impulse is dissipated, acoustic pressure waves converge to zero in the case of the G-Equation, as shown in figure 4 where the acoustics pressure p_{ref} was computed at the location x_{ref}. The same configuration is then simulated using the new model which includes hydrodynamics, and the results are shown in figure 4. The hydrodynamic simulation appears unstable, with a slow exponential growth.

The frequency responses of both the G-Equation and hydrodynamic models are shown in figure 5. With the G-Equation, the second acoustic mode bears the highest amplitude but is stable. In the hydrodynamic model, the second mode is still the highest amplitude mode, but now becomes unstable under the effects of the hydrodynamics on the flame.

The Darrieus-Landau instability causes a wrinkling of the flame front under the effects of deflected streamlines.[16] Wrinkling of the flame increases the surface area of the flame, and therefore the energy emitted by the flame. As such, wrinkling has the potential of changing the growth of the acoustic modes, and therefore the stability of the system as a whole. The plot of the fluctuating flame front for the hydrodynamic simulation is shown in figure 6, and shows this same wrinkling, characteristic of the Darrieus-Landau instability. The experiments conducted by Ref. 27 on the inverted v-flame show a similar wrinkling, but with an exponential growth of the flame wrinkles with increasing distance from the anchoring point. The fact that this exponential growth is not observed in our simulation could be explained by the different steady geometry used (v-flame vs. inverted v-flame in Ref. 27), or the presence of acoustic coupling. Wrinkling is not observed in G-Equation simulation, and so it is assumed that the instability of the system is due to the Darrieus-Landau instability.

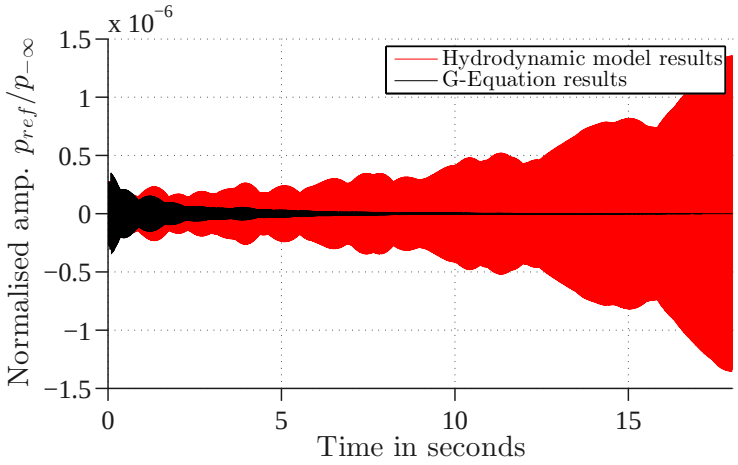

Figure 4. Comparison of the normalised pressure obtained from the G-Equation and hydrodynamic model in the stable case.

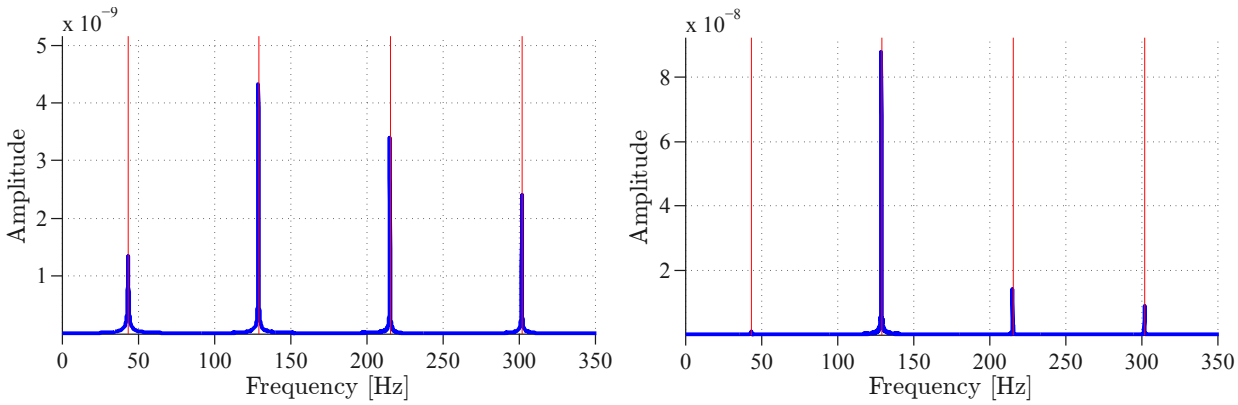

(a) G-Equation (b) New hydrodynamic model

Figure 5. Frequency responses in the stable case. The vertical red lines are the acoustic modes calculated analytically.

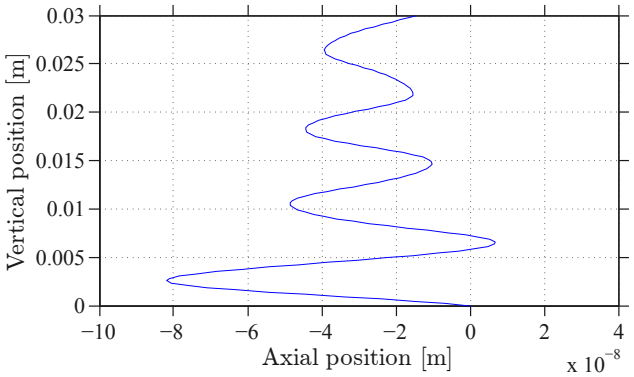

Figure 6. Fluctuating part of the flame front at t= 17s for the hydrodynamic model simulation in the stable case.

IV.B. Unstable Configuration

The length of the duct is now changed such that a flame-acoustic instability develops in the G-Equation simulation. The parameters for this new simulation are shown in table 2.

Table 2. Combustor parameters for the comparison to the G-Equation results in the unstable case.

$h/2$ [cm]	x_u[m]	x_d[m]	x_{ref}[m]	R_u	R_d	M	δx [mm]	δt [ms]	Flame angle [°]	$\bar{Q}/\theta_{-\infty}$
3	-1.0	0.75	0.118	1	-1	0.02	0.236	0.02	8.627	0.075

After an initial perturbation, the G-Equation shows an exponentially increasing normalised pressure amplitude, as seen in figure 7; it is expected that the amplitude will saturate later in time under the effects of non-linearity, but such behaviour will not be useful in our comparison and is therefore not shown. The growth rate of the instability is very low, as would be expected from such a low mean heat release. The new model including hydrodynamics is now run with the same parameters. The results show an unstable system with a growth rate comparable to the G-Equation, as shown in figure 7.

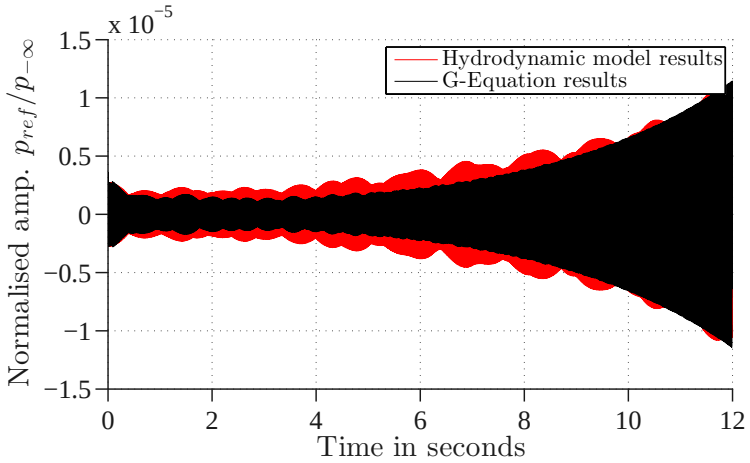

Figure 7. Comparison of the normalised pressure obtained from the G-Equation and hydrodynamic model in the unstable case.

Looking at the frequency responses of the two models, shown in figure 8, we can see that the G-Equation develops an instability at the first acoustic mode, whereas the Hydrodynamic model develops an instability at the second acoustic mode. It is assumed that the wrinkling of the flame obtained with the hydrodynamic model and shown in figure 9 is responsible for damping the instability around the first acoustic mode, and developing an instability around the second acoustic mode.

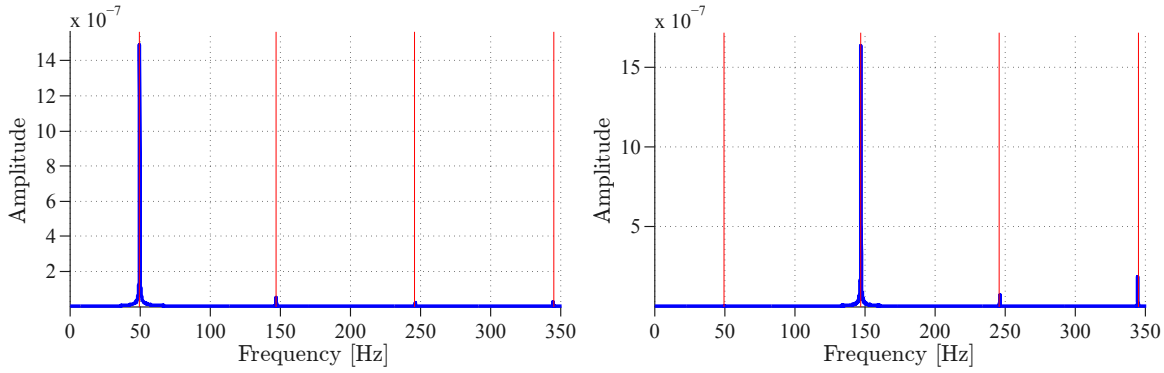

(a) G-Equation (b) New hydrodynamic model

Figure 8. Frequency responses in the unstable case. The vertical red lines are the acoustic modes calculated analytically.

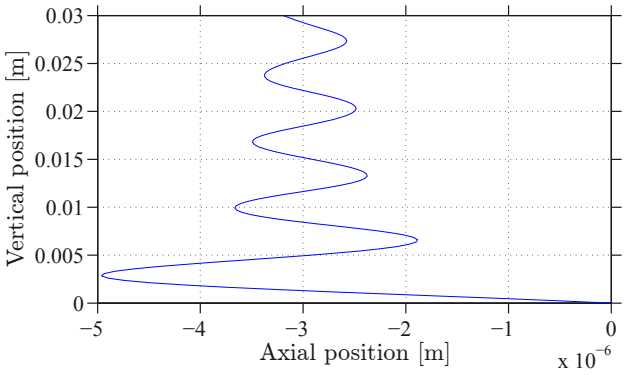

Figure 9. Fluctuating part of the flame front at time t= 17s for the hydrodynamic model simulation in the unstable case.

V. Conclusion

This paper has presented a new method for solving combustion instabilities including both acoustic and hydrodynamic flame coupling for an anchored V-flame configuration. The simulation results were compared to the G-Equation results, and showed a change in the frequency of the instability in the unstable case. In the stable case, the G-Equation simulations remained stable, whilst the hydrodynamic model developed an instability that we attribute the the Darrieus-Landau instability.

Preliminary results are encouraging, and capture phenomena commonly associated with Darrieus-Landau instabilities, such as the change of the oscillation frequency of the unstable mode, and the wrinkling of the flame. Further validation is required to verify the robustness of the numerical schemes used, and in particular verify the stability and error associated with the signal extension method. Furthermore, a thorough analysis of the Darrieus-Landau instability growth rates as a function of excitation wave-number must be conducted. This will be done by varying the length of the tube.

References

[1]Swaminathan, N. and Bray, K., *Turbulent Premixed Flames*, 2011.

[2]Lieuwen, T., "Modeling Premixed Combustion Acoustic Wave Interactions : A Review," *Journal of Propulsion and Power*, Vol. 19, No. 5, 2003, pp. 765–781.

[3]Rayleigh, J., *The Theory of Sound, Volume 2*, Dover Publications Inc., 1945.

[4]Haugen, N., Langø rgen, O., and Sannan, S., "Nonlinear simulations of combustion instabilities with a quasi-1D Navier-Stokes code," *Journal of Sound and Vibration*, Vol. 330, No. 23, Nov. 2011, pp. 5644–5659.

[5]Searby, G., "Experimental studies of instabilities of laminar premixed flames," *International Conference on Combustion and Detonation*, 2004, pp. 1–32.

[6]Matkowsky, B. and Sivashinsky, G., "An Asymptotic Derivation of Two Models in Flame Theory Associated with the Constant Density Approximation," *SIAM Journal on Applied Mathematics*, Vol. 37, No. 3, 1979, pp. 686.

[7]Matalon, M. and Matkowsky, B., "Flames as gasdynamic discontinuities," *Journal of Fluid Mechanics*, Vol. 124, April 1982, pp. 239–259.

[8]Wu, X., Wang, M., Moin, P., and Peters, N., "Combustion instability due to the nonlinear interaction between sound and flame," *Journal of Fluid Mechanics*, Vol. 497, Dec. 2003, pp. 23–53.

[9]Shanbhogue, S., Husain, S., and Lieuwen, T., "Lean blowoff of bluff body stabilized flames: Scaling and dynamics," *Progress in Energy and Combustion Science*, Vol. 35, Feb. 2009, pp. 98–120.

[10]Ebrahimi, H., "Overview of Gas Turbine Augmentor Design, operation And Combustion Oscillation," *Annual Conference on Liquid Atomization and Spray Systems*, No. May, 2006.

[11]Wu, X. and Moin, P., "Large-activation-energy theory for premixed combustion under the influence of enthalpy fluctuations," *Journal of Fluid Mechanics*, Vol. 655, May 2010, pp. 3–37.

[12]Altantzis, C., Frouzakis, C., Tomboulides, A., Matalon, M., and Boulouchos, K., "Hydrodynamic and thermodiffusive instability effects on the evolution of laminar planar lean premixed hydrogen flames," *Journal of Fluid Mechanics*, Vol. 700, May 2012, pp. 329–361.

[13]Dowling, A. P., "A kinematic model of a ducted flame," *Journal of Fluid Mechanics*, Vol. 394, Sept. 1999, pp. 51–72.

[14]Dowling, A. P., "Nonlinear self-excited oscillations of a ducted flame," *Journal of Fluid Mechanics*, Vol. 346, 1997, pp. 271–290.

[15]Wu, X. and Law, C., "Flame-acoustic resonance initiated by vortical disturbances," *Journal of Fluid Mechanics*, Vol. 634, Aug. 2009, pp. 321.

[16]Pelce, P. and Clavin, P., "Influence of hydrodynamics and diffusion upon the stability limits," *Journal of Fluid Mechanics*, Vol. 124, 1982, pp. 219–237.

[17]Mariappan, S. and Sujith, R. I., "Modelling nonlinear thermoacoustic instability in an electrically heated Rijke tube," *Journal of Fluid Mechanics*, Vol. 680, No. 2011, May 2011, pp. 511–533.

[18]Fleifil, M., Annaswamy, A. M., Ghoneim, Z. A., and Ghoniem, A. F., "Response of a Laminar Premixed Flame to Flow Oscillations : A Kinematic Model and Thermoacoustic Instability Results," *Combustion and Flame*, , No. 106, 1996, pp. 487–510.

[19]Dowling, A. P., "The calculation of thermoacoustic oscillations," *Journal of Sound and Vibration*, Vol. 180, No. 4, 1995, pp. 557–581.

[20]Langhorne, P. J., "Reheat buzz: an acoustically coupled combustion instability. Part 2. Theory," *Journal of Fluid Mechanics*, Vol. 193, April 1988, pp. 445–473.

[21]Shin, D., Plaks, D., Lieuwen, T., Mondragon, U., Brown, C., and McDonell, V., "Dynamics of a Longitudinally Forced, Bluff Body Stabilized Flame," *Journal of Propulsion and Power*, Vol. 27, No. 1, Jan. 2011, pp. 105–116.

[22]Clanet, C. and Searby, G., "First Experimental Study of the Darrieus-Landau Instability," *Physical Review Letters*, Vol. 80, No. 17, 1998, pp. 3867–3870.

[23]Assier, R. C. and Wu, X., "Linear and weakly non linear instability of a premixed curved flame under the influence of its spontaneous acoustic field," *Submitted to Journal of Fluid Mechanics*, 2013.

[24]Bruno, O. P., Han, Y., and Pohlman, M. M., "Accurate, high-order representation of complex three-dimensional surfaces via Fourier continuation analysis," *Journal of Computational Physics*, Vol. 227, No. 2, Dec. 2007, pp. 1094–1125.

[25]Candel, S., "Combustion Dynamics and Control: Progress and Challenges," *Proceedings of the Combustion Institute*, Vol. 29, 2002, pp. 1–28.

[26]Evesque, S., *Adaptive Control of Combustion Oscillations*, Ph.D. thesis, University of Cambridge, 2000.

[27]Truffaut, J. and Searby, G., "Experimental Study of the Darrieus-Landau instability on an inverted 'V'-flame, and measurement of the markstein number," *Combustion Science and Technology*, Vol. 149, 1999, pp. 35–52.